



Structural, microstructural, electrical, thermal and non-isothermal degradation kinetic studies on technologically important poly (aniline)/CdO nanocomposites

M. Amita¹ · K. Kiruthiga² · S. Mahalakshmi³ · V. Parthasarathy⁴ · Chechia Hu⁵ · Yi-Feng Lin⁵ · Kuo-Lun Tung⁶ · R. Anbarasan⁶

Received: 8 July 2018 / Accepted: 17 June 2019 / Published online: 5 July 2019
© Springer Science+Business Media, LLC, part of Springer Nature 2019

Abstract

The main aim of this study was to prepare polyaniline (PANI) nanocomposites. The CdO nanoparticles were obtained by the sol–gel method. The PANI-CdO nanocomposites were synthesized by in situ chemical oxidative polymerization technique. The chemical structure of CdO, PANI and PANI nanocomposites were confirmed by FTIR and XRD techniques. The surface morphology of CdO and PANI nanocomposites was investigated using SEM. The TEM analysis was used to confirm the actual particle size of the CdO nanoparticles. The morphology and surface roughness of the prepared composites were examined with the help of atomic force microscopy. The band gap values of PANI and PANI nanocomposites were determined using Tauc's plot. The thermal properties of PANI nanocomposites were assessed using thermogravimetric analysis. The non-isothermal degradation kinetic study was carried out to comprehend the degradation rate and determine the energy of activation (E_a). The dc electrical conductivity study was also carried out for the prepared composites.

Graphical Abstract

The non-isothermal degradation kinetics of PANI/CdO (10 weight % loaded) system was carried out under air atmosphere. It was found that while increasing the heating rate the degradation temperature of PANI was increased. The energy of activation for the degradation of PANI backbone was determined by using various kinetic models. It was found that the Kissinger model is an opt method to determine the E_a value for degradation.

✉ V. Parthasarathy
vpsarathy11dec@gmail.com

✉ Kuo-Lun Tung
kltung@ntu.edu.tw

¹ Department of Physics, Christ College of Science and Management, Sonnur 563160 Karnataka, India

² Department of Chemistry, Hindustan Institute of Technology and Science, Padur, 603 103 Chennai, Tamilnadu, India

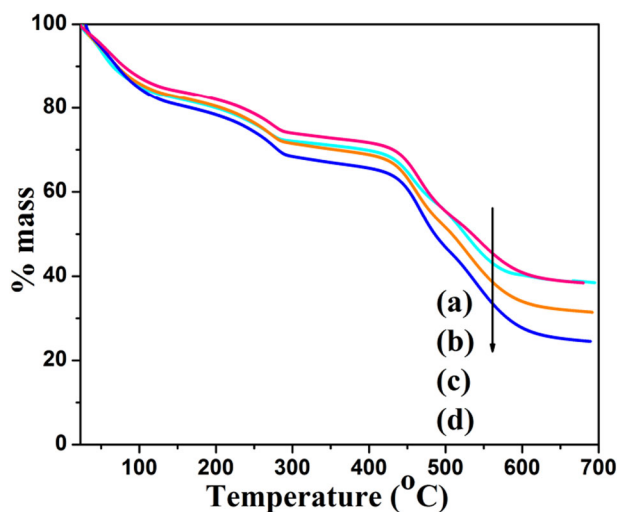
³ Department of Physics, Anand Institute of Higher Technology,

Kazhipattur, 603 103 Chennai, Tamilnadu, India

⁴ Department of Physics, Hindustan Institute of Technology and Science, Padur, 603 103 Chennai, Tamilnadu, India

⁵ Department of Chemical Engineering, Luh Hwa Research Centre for Circular Economy and R&D Centre for Membrane Technology, Chung Yuan Christian University, Taipei 32023, Taiwan

⁶ Department of Chemical Engineering, National Taiwan University, Taipei 10617, Taiwan



Highlights

- PANI-CdO nanocomposites were successfully prepared by chemical oxidative in situ polymerization technique.
- The FTIR spectrum confirmed that the PANI backbone was made by benzenoid and quinonoid units.
- The average grain size of CdO was found to be 42 nm.
- The degradation temperature (T_d) of PANI nanocomposites was increased gradually in accordance with the heating rates.
- The energy of activation for the degradation process was calculated under non-isothermal condition using various kinetic models. The Kissinger model exhibited the opt energy of activation for the degradation process.

Keywords PANI · Band gap · Benzenoid and quinoid structure · Degradation kinetics · AFM · TGA

1 Introduction

Conducting polymers (CPs) have received much more attention among the researchers owing to their technological importance in rechargeable batteries, organic photovoltaic cells, supercapacitors, electroluminescent devices, chemical sensors, aircraft structures and polymer based electronic and optoelectronic devices [1]. They have alternative single and double bonds conjugation resulting with charge delocalization along the entire polymer chain. The current conduction occurs in CPs is only through charge delocalization. The electrical properties of these polymers can be altered by the partial oxidation or reduction of the polymer chain during the doping or de-doping process. CPs such as poly(pyrrole), poly(thiophene), poly(aniline), poly(acetylene), poly(p-phenylene), and their derivatives have been studied for their potential applications [2–4]. Among these polymers, poly(aniline) (PANI) is a well-known electrically CP studied for its good stability, good conductivity, facile synthesis, electrochromic behaviour, acid-base properties and good processability [5, 6]. It is used in sensors, batteries, electronic devices, and corrosion protection in organic coatings [7–9]. The addition of nano-sized inorganic fillers will enhance the electrical and microscopic

properties of PANI [10]. Hence, the preparation of polymer/inorganic hybrid structure is one of the ideal ways to obtain new composite materials with the synergetic properties of both polymer and an inorganic filler. The PANI/TiO₂ nanocomposite was studied by Balaz and his research team in the year 2006 [11]. The PANI/NiFe₃O₄/graphite nanocomposite has microwave absorbing property [12]. PANI magnetic nanocomposite film was analyzed by XRD, UV visible spectrometry, TEM and conductivity measurement [13]. Liu et al. [14] reported that the thermal stability of polyaniline was increased after dispersing some Cu nanoparticles in the polymer matrix. The structural properties of PANI-CdS nanocomposite were studied with FITR, XRD and TEM by Ingle and his co-workers in the year 2014 [15]. The dc conductivity and thermal stability of PANI tungsten oxide nanocomposite were analyzed by Sastry and his research team [16]. It revealed that the thermal stability of PANI composites improved when compared with pristine PANI due to the incorporation of tungsten oxide in the PANI matrix. Researchers are interested in preparing polymer composites using metal oxides as they possess remarkable optical, physical and chemical properties. The incorporation of such nanofillers into PANI matrix will facilitate the synergistic effect between the constituents.

CdO is an n-type semiconductor with the direct band gap of 2.2 eV to 2.5 eV and is used as transparent conductive oxides. It is mainly used in solar cells [17], diodes and transparent electrodes [18] as it has high transparency in the visible region of solar spectrum. CdO has been selected for this work to prepare PANI nanocomposites due to its low resistivity and good optical transparency as well as its gas sensing performance. Aashis et al. [19] reported that the ac conductivity of PANI nanocomposite increased while increasing the concentration of CdO in PANI. The thermal stability of different metal oxide doped PANI was reported in the literature [20]. The understanding of thermal stability and thermal degradation behaviour under the non-isothermal condition is more important for processing, thermal recycling, and applications for any types of polymers. The available literature revealed that there was no report on the thermal degradation kinetics of PANI nanocomposites. This urged us to do the present investigation. This type of composite will be used as a gas sensor to detect various gases based on its change in resistivity as well as in optoelectronic devices due to its semiconducting nature.

2 Experimental

2.1 Materials

Aniline (ANI, monomer) was procured from S.D. fine chemical, India. It was purified prior to polymerization reaction by distillation to remove the impurities present in the monomer. All other chemicals required for this work were used as received. Cadmium acetate dihydrate and sodium hydroxide were supplied by Ottokemi, India. Hydrochloric acid (HCl) and ammonium peroxydisulphate (PDS) were purchased from Reachem, India. Double distilled water (DDW) was used for making solutions.

2.2 Preparation of CdO nanoparticles

Cadmium acetate dihydrate was used as a starting material to prepare cadmium oxide nanoparticles. The low cost sol-gel technique has been employed for the preparation of nanoparticles. A predetermined amount of cadmium acetate was separately dissolved in 100 mL of distilled water. Then, ammonium hydroxide solution was added dropwise into the above mentioned solution till pH reaches 8. The obtained homogeneous gel was separated by filtration. Afterward, it was dried overnight in an oven at 100 °C. Thus obtained cadmium hydroxide was grounded as a fine powder using mortar and pestle. The resultant powder was kept in a

furnace at 400 °C for 2 h to get CdO nanoparticles. The obtained powder was brown in colour.

2.3 Preparation of PANI and PANI-CdO nanocomposites

PANI was prepared by polymerization of ANI using HCl as a dopant and PDS as an oxidant by the chemical oxidative polymerization technique. Ten millilitres of 1 M ANI was taken in a 250 mL capacity round bottomed flask maintained at 0–5 °C under N₂ atmosphere. 0.50 g PDS was dissolved separately in 5 mL of 1 M HCl solution, and that was added to the above said solution with vigorous stirring to initiate the polymerization reaction. The temperature was maintained at 0–5 °C until the completion of the polymerization reaction. The polymerization took place with the visible appearance of green colour during this process. The polymerization is continued for further 2 h. The obtained green precipitate was filtered using G4 sintered crucible and washed many times with 1 M HCl followed by distilled water till the filtrate becomes colourless. Finally, the precipitate was washed with excess ethanol to remove the unreacted monomer and dried at 65 °C for 6 h. Thus prepared PANI was weighed and stored in a zipper lock cover. The same method was adopted for the preparation of PANI/CdO nanocomposites in the presence of different % weight loading of CdO nanoparticles such as 5, 10 and 15 weight %. The in situ polymerization technique was adopted for the preparation of PANI/CdO nanocomposites. As mentioned above, 10 mL monomer and 5 mL PDS solutions were taken in a 250 mL round bottomed flask. With this 5% weight of CdO nanoparticles (for instance) was taken and stirred well at 0–5 °C under inert atmosphere. After 2 h of polymerization reaction, the dark coloured precipitate was filtered using G4 sintered crucible and washed three times with excess amount of ethanol. The precipitate was dried at 65 °C for 6 h. Thus obtained PANI/CdO nanocomposite was weighed and stored in a zipper lock cover under nitrogen atmosphere to avoid oxidation by air.

2.4 Characterization

All the prepared samples were analyzed using various analytical tools to assess their structure and properties. FTIR spectra of prepared CdO nanoparticles and PANI-CdO nanocomposites were taken using Shimadzu 8400S FTIR spectrophotometer by KBr pelletization method. To record FTIR spectrum, 10 mg of sample was mixed with KBr, and that was grinded together using mortar and pestle. The finely grinded powder was made as a thin film to record the spectrum. The structure of the nanoparticles and polymer nanocomposites was further confirmed by X-ray

diffractometer (Bruker K 8600) using the $\text{CuK}\alpha$ ($\lambda = 1.5405 \text{ \AA}$) radiation. The particle size of the CdO nanoparticles was estimated by Scherrer's formula [21].

$$d = \frac{0.94 \lambda}{\beta \cos \theta} \quad (1)$$

where β represents the full width half maximum (FWHM), θ is the diffraction angle, d describes the average grain size and λ denotes the wavelength of X-rays.

The optical properties of nano-sized CdO and PANI nanocomposites can be analyzed using UV–visible spectroscopy. The UV–vis spectra were recorded for all the prepared samples using UV-1800 Shimadzu double beam spectrometer. The energy bandgap of the nano-sized CdO, PANI and PANI composites can be determined using Tauc's relation [22]:

$$(\alpha h\nu)^{1/n} = A(h\nu - E_g) \quad (2)$$

where α represents the absorption coefficient, E_g is the bandgap energy, $h\nu$ is the energy of photon and the exponent n takes different values such as 1/2, 3/2, 2 and 3 for direct allowed, direct forbidden, indirect allowed and indirect forbidden transitions respectively [21].

The morphology of the nanoparticles and polymer nanocomposites was investigated using SEM (JEOL JSM 5610 LV). The actual particle size and the crystalline nature of the as prepared CdO nanoparticles can be assessed using JEOL 2100 transmission electron microscope (TEM). Fifty milligrams of PANI/CdO nanocomposite sample was made as a thin sheet by applying the pressure of 7 tons. Afterwards, it was gold coated under vacuum prior to SEM analysis. The thermal stability of pure PANI and PANI nanocomposites was analyzed using TG/DTA 6200 thermal analyser in the temperature range of 30–700 °C at four different heating rates from 10 °C/min to 25 °C/min in steps of 5 °C/min under air atmosphere.

The conductivity measurement was also performed for the polymer and polymer nanocomposites using two probe method. The powder samples were pelletized by using the hydraulic press to carry out this analysis. The electrical conductivity was measured using the following expression,

$$\sigma_{dc} = \frac{d}{RA} (\text{S/cm}) \quad (3)$$

where $A = 2.25 \text{ cm}^2$ is the area of the silver electrode, d denotes the thickness of the prepared pellet and R its resistance.

2.5 Non-isothermal degradation kinetics

The non-isothermal degradation kinetic studies for the prepared PANI nanocomposites were assessed by using

three kinetic models such as Flynn-Wall-Ozawa (FWO), Kissinger and Auggis-Bennet models [23]. The reaction conversion (α) is determined using the following equation:

$$\alpha = W_o - W_t / W_o - W_f \quad (4)$$

where W_o is the initial weight, W_f is the weight at the end of the process and W_t is the weight at a particular temperature.

2.5.1 FWO method

The degradation of materials can be studied under dynamic conditions by using the FWO method [23]. It is one of the most used models which gives more accurate results without any assumptions. This model proposes the following mathematical expression to estimate the activation energy,

$$E_a = \frac{-R}{1.052} \times \frac{\Delta\lambda\nu\beta}{\Delta(\frac{1}{T})} \quad (5)$$

where E_a is activation energy, R refers to the gas constant, β describes the heating rate and T is the temperature. The E_a can be determined from the slope of the plot, β vs $1/T$.

2.5.2 Kissinger model

The Kissinger model [23] is one of the important classical kinetic models. The reaction rate is high at the thermal degradation temperature (T_d) according to this model. The degree of conversion (α) at T_d is constant, but it varies with the heating rate. The Kissinger model based equation is given as follows:

$$\ln\left(\frac{\beta}{T_d^2}\right) = \ln\left(\frac{AR}{E}\right) - \frac{E}{RT_d} \quad (6)$$

The plot of $\ln(\beta/T_d^2)$ vs $1/T_d$ is used to determine E_a by this method.

2.5.3 Auggis-Bennet model

Auggis and Bennet [23] proposed this classical kinetic model in order to evaluate activation energy during the degradation process which is given as follows:

$$\ln\left(\frac{\beta}{T_d}\right) = -\frac{E}{RT_d} + \ln A \quad (7)$$

where T_d is the degradation temperature, and that can be measured from the thermal analysis curve. The E_a value is determined from the slope of the straight line plot, $\ln(\beta/T_d)$ vs $1/T_d$.

2.5.4 Friedman method

Friedman method [23] is an iso-conversional method which proposes the following mathematical expression based on

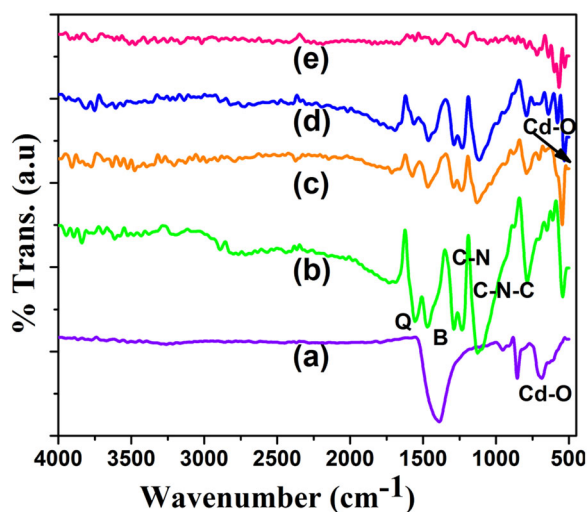


Fig. 1 FTIR spectrum of **a** CdO, **b** PANI, **c** PANI loaded with 5% weight CdO, **d** PANI loaded with 10% weight CdO, **e** PANI loaded with 15% weight CdO

Arrhenius equation to analyse the thermal degradation kinetic studies:

$$\ln\left(\frac{d\alpha}{dt}\right) = \ln(Z) + n \ln(1 - \alpha) - \frac{E_a}{R_1 T} \quad (8)$$

where α is the conversion rate at time t , T is the temperature and R is the gas constant. The E_a values can be obtained at different stages of the degradation process.

3 Results and discussion

3.1 FTIR study

FTIR measurement was carried out to confirm the chemical structure of prepared CdO nanoparticle and PANI nanocomposites. Figure 1a shows the FTIR spectrum of nano-sized CdO. The spectrum has shown three well defined peaks. The appearance of a broad peak at 1389 cm^{-1} is attributed to wagging vibration of CdO. The peaks assigned at 855 cm^{-1} and 682 cm^{-1} are associated with the stretching vibration of nano-sized CdO [21]. Figure 1b–e displays the FTIR spectra of pure PANI and PANI–CdO nanocomposites. The N–H stretching of aromatic amine is noticed at 3426 cm^{-1} . The aromatic C–H stretching vibration is seen at 2894 cm^{-1} . The benzenoid and quinoid stretchings are assigned at 1466 cm^{-1} and 1556 cm^{-1} respectively. These peaks are used to confirm the formation of PANI structure. The C–N stretching is noticed at 1285 cm^{-1} . The peak assigned at 1225 cm^{-1} is linked with the polaronic structure of PANI. The C–N–C stretching and C–H in-plane bending vibrations are observed at 1114 cm^{-1} and 772 cm^{-1} respectively. The peaks of PANI-composites shifted

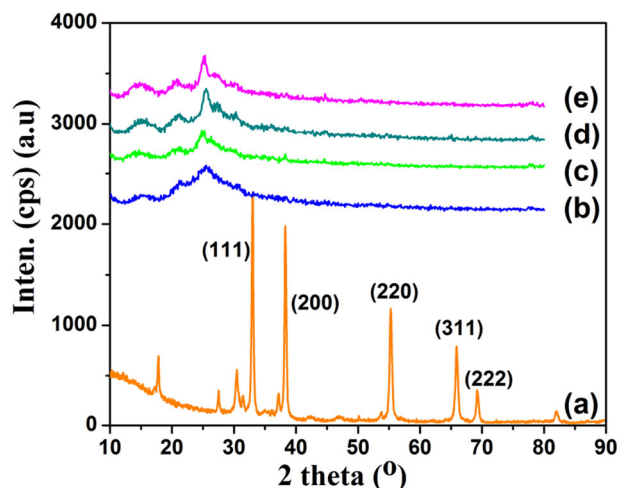


Fig. 2 XRD of **a** CdO, **b** PANI, **c** PANI loaded with 5% weight CdO, **d** PANI loaded with 10% weight CdO, **e** PANI loaded with 15% weight CdO

towards higher wavenumber when compared with pure PANI. This authentically confirms the interaction of CdO with PANI matrix. The Cd–O stretching peak is seen at 651 cm^{-1} in the FTIR spectra of PANI nanocomposites which also confirmed the interaction of CdO with PANI [24]. The blue shift in the metal oxide stretching peak confirmed the above said statement.

3.2 XRD analysis

The crystalline nature of the prepared samples was further confirmed by X-ray diffraction technique. The XRD profile of nano-sized CdO is shown in Fig. 2a. It revealed that CdO nanopowder is highly crystalline. The diffraction peaks observed at the 2θ values of 32.8° , 39.2° , 55° , 65° , and 69.5° correspond to (111), (200), (220), (311) and (222) crystalline planes of CdO nanoparticles respectively. These peaks are in good agreement with the standard JCPDS data (File no. 05-0640). It further confirms the cubic phase of CdO. The particle size of the prepared CdO was calculated using Scherrer's formula (Eq. 1). The average particle size of CdO was estimated as 42 nm. The remarkably broadened reflection peaks also supported that the particles are in the nano range. Further, the size of CdO will be confirmed by TEM measurement. The XRD patterns of pure PANI and 5, 10 and 15 weight % of CdO doped PANI nanocomposites are illustrated in Fig. 2b–e. A broad peak observed at $2\theta = 25.01^\circ$ [25] in the XRD profiles of pure PANI and its composites which indicates the amorphous nature of PANI. It was noted that the sharpness of the amorphous peaks increases with the increasing concentration of CdO loading in PANI. It means that the overall crystallinity of PANI/CdO nanocomposites has been increased while increasing the % weight loading of CdO. It is authentically proved that

CdO has been successfully incorporated into PANI matrix which has also enhanced the crystallinity of amorphous PANI as CdO is highly crystalline. It also confirmed the presence of CdO in PANI matrix. Aldwayyan et al. [26] explained that CdO is a poly crystalline material and the same can act as a template for the growth of polymer chains [27]. In the present work, PANI/CdO nanocomposites are prepared by in situ method. Hence, there is a chance to grow the polymer chains in the basal spacing of the CdO nanoparticles. This leads to the stereo regular arrangement of PANI chains. The next possibility is the growing of PANI chains on the surface of the CdO nanoparticles. At the same time the content of crystalline CdO is increased. As a result, the crystallinity of PANI chains can be increased slightly. That's why while increasing the % weight loading of CdO nanoparticles, the crystallinity of the polymer/nanocomposites are increased.

3.3 Optical studies

3.3.1 UV-visible spectral study

The absorption coefficient and optical bandgap of the materials are the most important factors to judge their optical characteristics and practical applications. Figure 3 demonstrates a UV–visible spectrum of nano-sized CdO. It shows a peak around 470 nm which corresponds to exciton transition from HOMO of valence band to LUMO of conduction band. The UV–visible spectra of pure PANI and 5, 10 and 15 weight % of CdO doped PANI nanocomposites are shown in Fig. 3b–e. Two well defined characteristics absorption bands are noticed in the UV–visible spectrum of pure PANI at 318 nm and 608 nm which are related to $\pi-\pi^*$ transition of the benzenoid ring and $\pi-\pi^*$ transition of benzenoid to quinoid excitonic transition respectively [28].

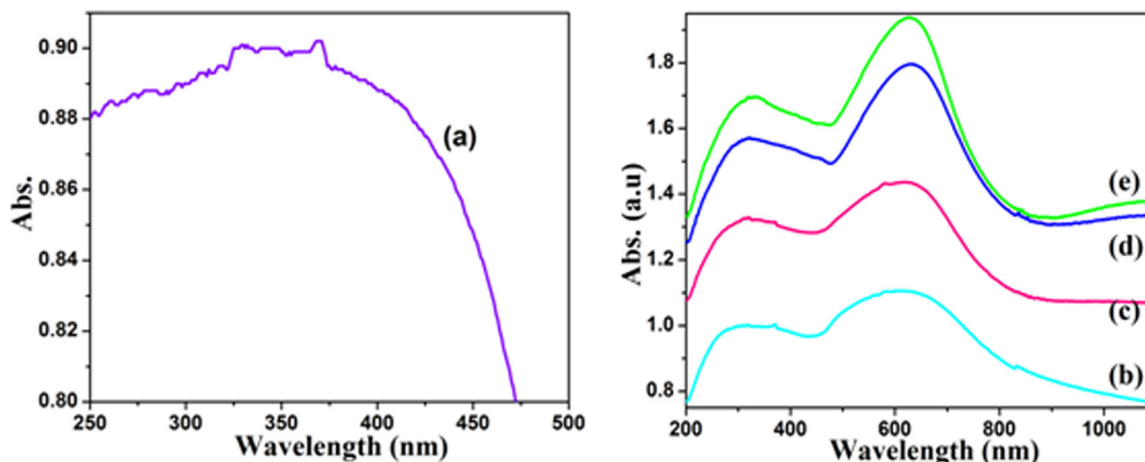


Fig. 3 UV–visible spectra of **a** CdO, **b** PANI, **c** PANI loaded with 5% weight CdO, **d** PANI loaded with 10% weight CdO, **e** PANI loaded with 15% weight CdO

One can observe significant changes in the absorption spectrum of PANI after incorporating nano-sized CdO into PANI matrix. The absorption spectra also revealed that PANI/CdO nanocomposites are in the electrically conducting state.

3.3.2 Determination of optical bandgap

The energy band gap (E_g) values of CdO nanoparticles, PANI and its composites were accurately determined using Eq. (2). The plot of $(\alpha h\nu)^2$ vs. $h\nu$ was made to determine the direct band gap value of CdO nanoparticles as shown in Fig. 4a (Table 1). The bandgap value of CdO was found to be 2.33 eV from the obtained plot. The obtained bandgap value is larger when compared with bulk CdO. The blue shift in the bandgap value confirms the size quantization

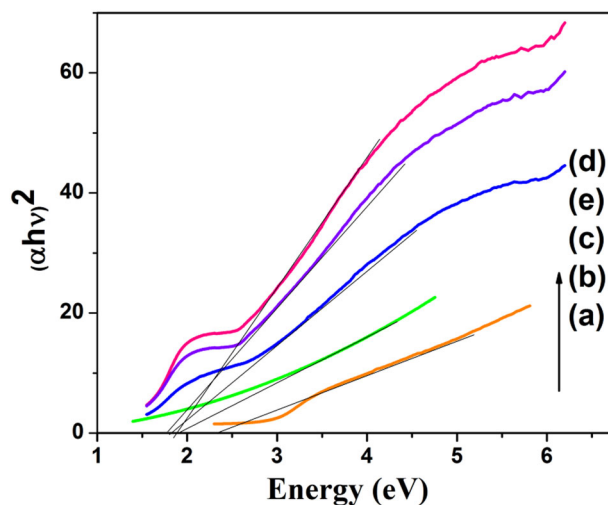


Fig. 4 Tauc's plot for **a** CdO, **b** PANI, **c** PANI loaded with 5% weight CdO, **d** PANI loaded with 10% weight CdO, **e** PANI loaded with 15% weight CdO

effect in CdO. The size dependent bandgap widening can be explained based on quantum confinement regimes [29]. Strong quantum confinement is possible when the size of the nanostructures is much smaller than Bohr radius [30]. While in the weak confinement, quantum effects occur due to the quantization of exciton motion [31]. Hence, the band gap shift is smaller than strong confinement. It is proved that the widening of band gap in CdO nanoparticles is due

to weak confinement since its particle size is higher than the Bohr radius of CdO. The plot of $(\alpha h\nu)^2$ vs. $h\nu$ was also made to estimate the band gap values for direct transition of pure PANI and CdO doped PANI nanocomposites as shown in Fig. 4b, c–e) respectively. The band gap values of pure PANI and its composites are presented in Table 1. The band gap of PANI nanocomposites gradually decreases in accordance with the increasing % weight of CdO in PANI. This is due to the creation of new energy levels in the band gap of PANI which enables the charge carriers to make transition from the valence band to the intermediate levels and then to the conduction band.

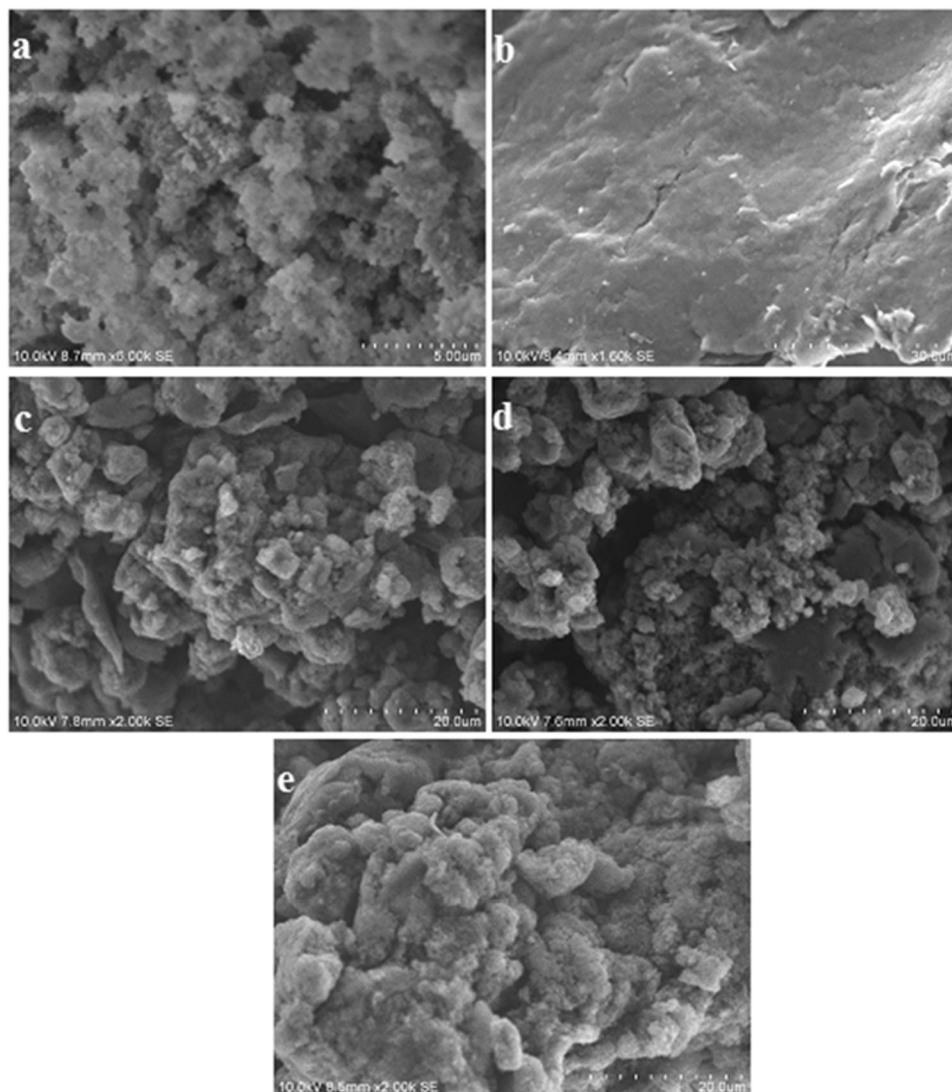
Table 1 E_g and DC conductivity values

System	E_g values (eV)	DC conductivity (S/cm)
CdO	2.32	–
PANI	1.93	4.72×10^{-4}
PANI-5% weight CdO	1.88	3.80×10^{-3}
PANI-10% weight CdO	1.85	2.68×10^{-2}
PANI-15% weight CdO	1.78	7.43×10^{-2}

3.4 SEM report

The SEM image of CdO nanoparticles is shown in Fig. 5a. The particles were seen to be agglomerated and there is no distinguished grain in the micrograph. The SEM

Fig. 5 SEM image of **a** CdO, **b** PANI, **c** PANI loaded with 5% weight CdO, **d** PANI loaded with 10% weight CdO, **e** PANI loaded with 15% weight CdO



micrograph exhibits sponge-like morphology in which particles are irregular in shape. Moreover, the CdO particles seem to be fluffy in the SEM illustration with the porous structure. Figure 5b depicts the SEM image of pure PANI. It shows micrometre sized irregular sheet-like morphology with some cracks. The surface of pure PANI seems to be rough. The SEM image of 5, 10 and 15 weight % CdO doped PANI nanocomposites are shown in Fig. 5c–e. The sheet-like morphology of PANI micrographs has been changed apparently after incorporating nano-sized CdO. The change in morphology of PANI proved the presence of CdO in PANI matrix. The SEM images of PANI nanocomposites exhibit a kind of fluffy like morphology with the porous structure. The change in morphology will help the transportation of charged particles through the carbon backbone of polymer chains [32]. The grains can be distinguished well in the micrographs of PANI composites.

3.5 TEM and AFM analysis

Figure 6a illustrates the TEM image of CdO nanoparticles. The morphology of the particles is irregular in

shape [33]. The size of the prepared CdO nanoparticles is in the range of 10–45 nm. The SEM and TEM reports are not matching with each other. It is important to note that the nanosized CdO is dispersed on the micrometer sized PANI matrix. Since TEM report gives more accurate information rather than SEM. The TEM image specifically focused on the image of CdO nanoparticles dispersed on the PANI matrix. The SAED pattern of CdO nanoparticles is shown in Fig. 6b. It shows the well organized concentric circular rings which confirm the crystalline nature of nano-sized CdO. Therefore, the TEM result is also in line with the XRD results. The AFM images of PANI and 5, 10 and 15 weight % of CdO doped PANI nanocomposites are shown in Fig. 6c–f. Root mean square (RMS) and surface roughness were measured from the AFM data. It was obtained as 17 nm for pure PANI, 29 nm for 5 weight % CdO, 33 nm for 10 weight % CdO and 34.6 nm for 15 weight % CdO doped PANI nanocomposites. The surface of the composites becomes more rough while increasing the CdO concentration in the PANI matrix. It was observed that the grains possess different sizes, shapes, and separation.

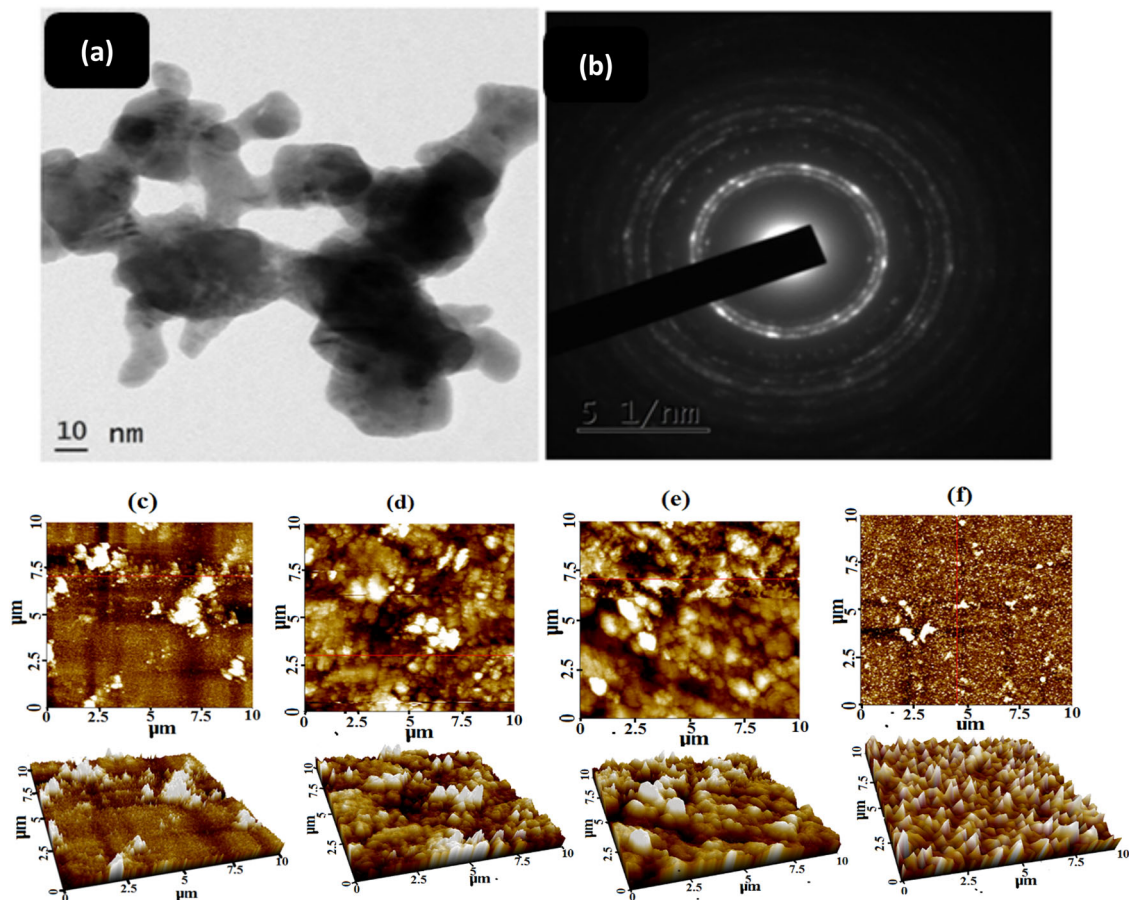


Fig. 6 a TEM image of CdO nanoparticles, b SAED pattern of CdO nanoparticles, AFM images of c PANI, d PANI-5% weight CdO, e PANI-10% weight CdO, f PANI-15% weight CdO

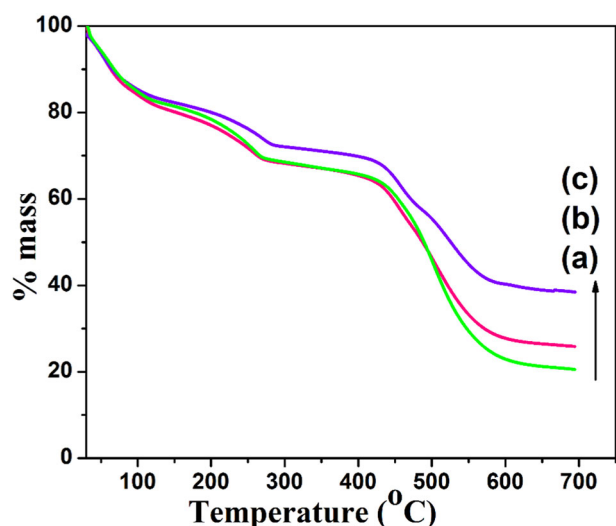


Fig. 7 TG thermogram of **a** PANI-5% weight CdO, **b** PANI-10% weight CdO, **c** PANI-15% weight CdO

3.6 TGA report

The thermal stability of the prepared PANI-CdO nanocomposites was assessed using TGA. The TG thermograms of PANI loaded with 5, 10 and 15 weight % of CdO loaded systems heated at 10 °C/min are shown in Fig. 7a–c. All the thermograms exhibit four steps degradation processes. The first minor weight loss step occurred below 100 °C is due to the removal of physisorbed water molecules and moisture [12]. The second minor weight loss around 190 °C is associated with the removal of HCl dopant from the benzenoid structure of PANI. The third minor weight loss step around 495 °C is associated with the oxidation of Cd(OH)₂ trace which present in CdO. Fourth major weight loss step at 509 °C is due to the degradation of the PANI backbone. This is in accordance with the recent literature report of HCl doped PANI by Daikh et al. [34]. The weight % residue remained above 600 °C was increased while increasing the CdO concentration in PANI. The thermal stability of PANI/CdO nanocomposites increased due to the addition of CdO nanoparticles. This can be explained as follows. During the in situ polymerization reaction, the PANI chains may be intercalated into the layered structure of CdO nanoparticles. As a result, the polymer chains are protected through umbrella effect. The weight % residue remained above 600 °C is associated with the char formation and CdO or Cd(OH)₂ nanoparticles loaded in PANI backbone. Anyhow, the main aim of the present study is not analysing the residue retained above 600 °C.

3.7 Non-isothermal degradation kinetic study

The non-isothermal degradation kinetic study was employed to estimate the activation energy (E_a) for the prepared PANI loaded with 10 weight % CdO

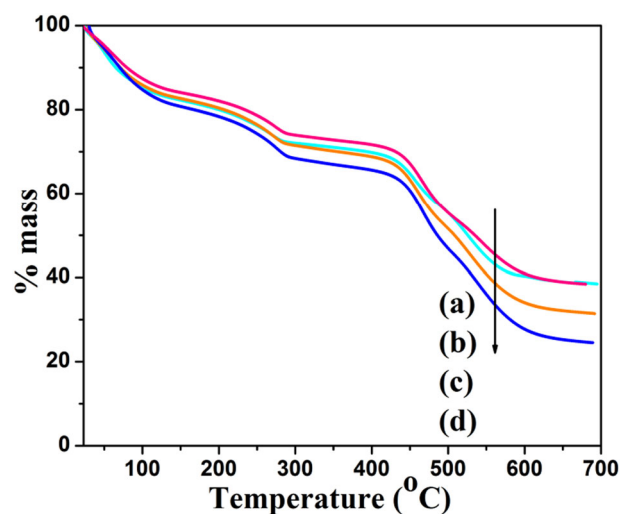


Fig. 8 TG thermogram of PANI-10% weight CdO nanocomposite system recorded at the different heating rates of **a** 10 °C/min, **b** 15 °C/min, **c** 20 °C/min, **d** 25 °C/min

nanocomposite system. For this purpose, various kinetic models were employed. The sample was heated at four different heating rates such as 10, 15, 20 and 25 °C/min to understand its degradation behaviour accurately. The TG thermograms of PANI loaded with 10 weight % CdO nanocomposite is shown in Fig. 8a–d. All the thermograms exhibited a four-step degradation processes as explained in the previous section. Moreover, the degradation steps shift towards higher temperature with the increase in heating rates. The plot of degradation temperature (T_d) vs. heating rates for all the three degradation steps is shown in Fig. 9a–c. It was also found that the T_d increases with the increasing heating rates for all the three degradation processes. This is due to the fast scanning process.

Non-isothermal degradation kinetic models are used to determine the E_a for the degradation of PANI nanocomposites where the maximum degradation occurred during their heating process. The plot of $\ln(\beta)$ vs. $1000/T_d$ was made to find out E_a by Flynnwall Ozawa model for all the three stages as shown in Fig. 9d, g, j. It was found to be 68.7 kJ mol⁻¹ for stage-I. The plot of $\ln(\beta/T_d)$ vs. $1000/T_d$ was made for Auggis-Bennet model to determine E_a for all the three stages as given in Fig. 9e, h, k. The E_a value was estimated as 59.2 kJ mol⁻¹ for stage-I. The plot of $(\ln(\beta/T_d^2))$ vs. $1000/T_d$ was made for Kissinger model for three stages as shown in Fig. 9f, i, l. The E_a value was calculated as 49.7 kJ mol⁻¹ for stage-I. By the linear fit method, the E_a values were determined for all the three stages of degradation for PANI/CdO nanocomposite system. The estimated E_a values of stage II and III by various models are listed in Table 2. Based on the amount of energy consumed, it was concluded that the stage-III consumed more amount of energy for the degradation of PANI backbone. This is true

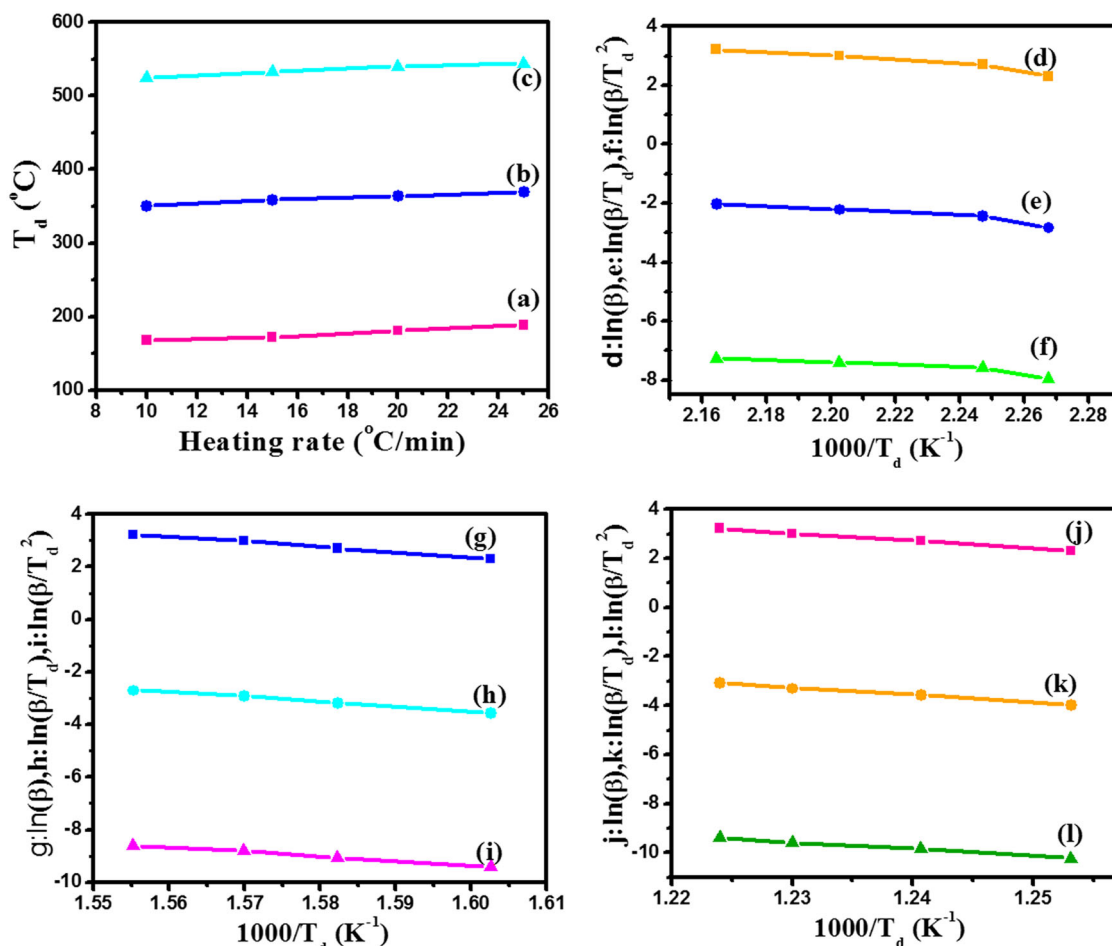


Fig. 9 The plot of heating rates vs. T_d : **a** stage-I, **b** stage-II, **c** stage-III. **d, g, j** Flynn-Wall-Ozawa model, **e, h, k** Auggis-Bennet model, **f, i, l** Kissinger model for stage-I, stage-II and stage-III respectively for PANI/CdO-10 weight % system

Table 2 E_a values from various models

Model	E_a values (kJ/mol)		
	Stage-I	Stage-II	Stage-III
FWO	68.7	133.6	236.5
Auggis-Bennet	59.2	114.3	226.3
Kissinger	49.7	95.1	206.2
Friedman (max)	21.6	66.5	180.3

because the removal of physisorbed water molecules or the removal of dopant HCl from the PANI backbone consumed lesser amount of energy. Moreover, the PANI backbone contains benzenoid and quinonoid rings, so that the third stage consumed more amount of thermal energy for its degradation. The E_a value obtained by Kissinger method was found to be low for all the three stages while comparing with the other two models. This is due to the denominator on Y-axis caption.

The E_a for the degradation of PANI/CdO nanocomposite system was also estimated by Friedman method (Table 2).

The E_a was calculated from the plot of $\ln(d\alpha/dt)$ vs. $1/T$ for all the three degradation stages by this method as shown in Figs. 10a–d, 10e–h and 10i–l respectively. All the plots exhibited a decreasing trend with respect to increase in heating rates [35]. The E_a values were found to be in the range of 11.3–21.6 kJ mol⁻¹ for the first stage, 31.6–66.5 kJ mol⁻¹ for the second stage and 116.3–180.3 kJ mol⁻¹ for the third stage degradation processes by the linear fit method. Further, the obtained E_a values were plotted against reaction extent (α) as shown in Fig. 10m–p. The results revealed that the E_a values increased gradually in accordance with the degradation steps. Generally, the E_a value increases up to the value of 0.5 [34], afterward there is a sudden increase in E_a value.

3.8 DC conductivity

The variation of dc electrical conductivity as a function of different weight % loading of nano-sized CdO in PANI matrix is shown in Fig. 11. The electrical conductivity of

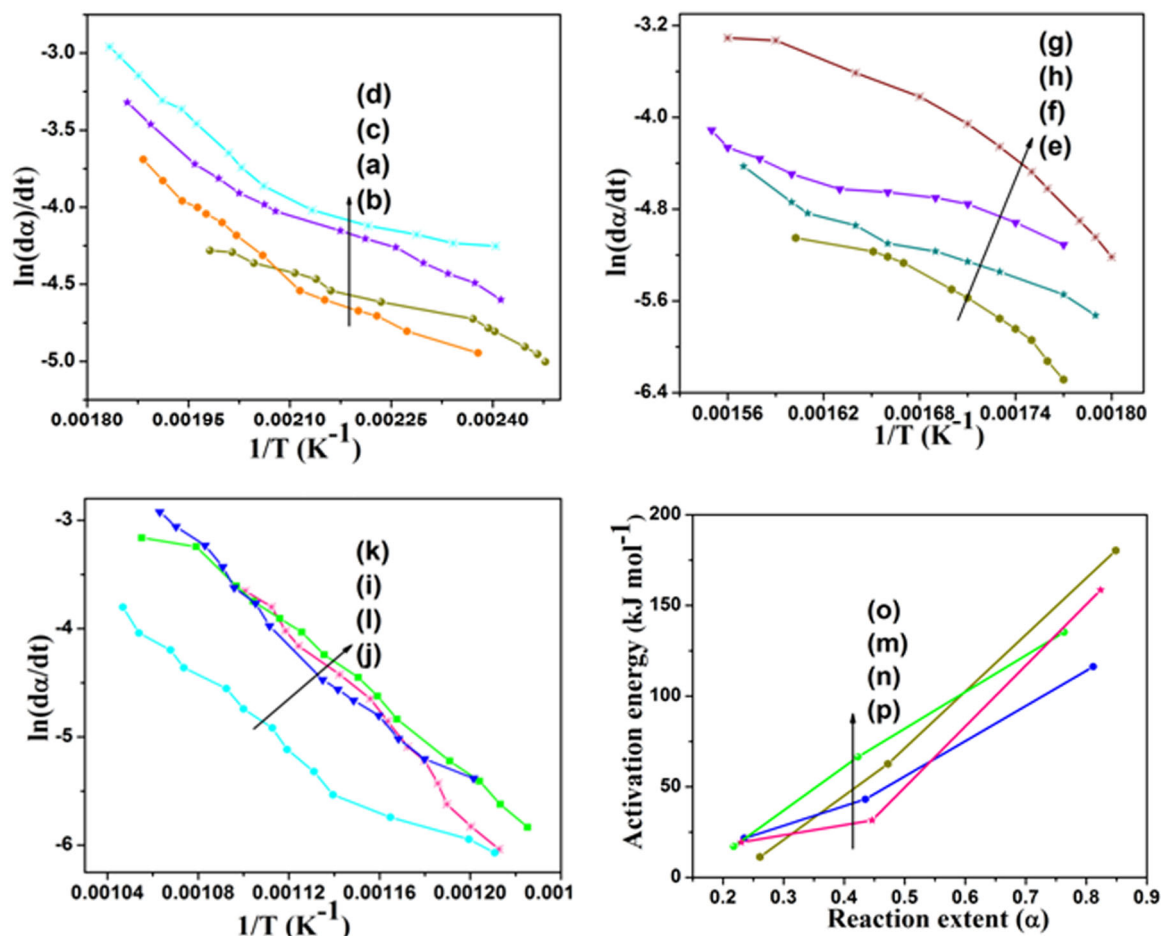


Fig. 10 The Friedman plot for a–d stage-I, e–h stage-II, i–l stage-III, m–p plot of E_a against Reaction extent for PANI/CdO-10% weight system

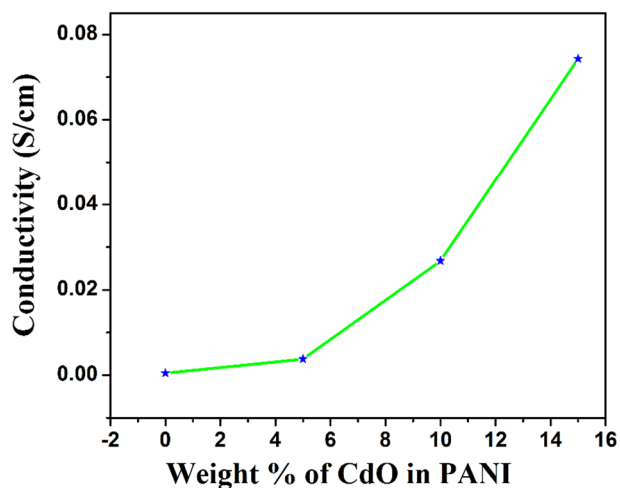


Fig. 11 Plot of weight % of CdO against conductivity of PANI system

PANI and its composites was observed to be in the semi-conducting range. Moreover, it was found that the dc conductivity of the prepared polymer nanocomposites increases

with the increasing CdO concentration. The reason for the increase in conductivity of PANI is due to the introduction of mobile charge carriers into the π -electronic system of PANI. The dc electrical conductivity values of PANI and its composites are listed in Table 1.

4 Conclusion

The PANI-CdO nanocomposites were successfully prepared by in situ chemical polymerization of aniline by varying the concentration of CdO nanoparticles. The presence of benzenoid (1466 cm^{-1}) and quinoid stretching vibrations (1556 cm^{-1}) in the FTIR spectra were used to confirm the chemical structure of PANI. The peak assigned at 651 cm^{-1} confirmed the interaction of CdO with PANI matrix. The structure and crystalline nature of pure CdO were confirmed by XRD pattern. The chemical interaction of CdO with PANI matrix was also confirmed by the presence of less intense sharp peaks in the XRD patterns of PANI nanocomposites. The particle size of CdO was determined as

42 nm and is also confirmed with TEM. The RMS and surface roughness of PANI/CdO nanocomposites were determined using AFM. The TG thermogram showed three step degradation processes. Moreover, the weight % residue remained above 700 °C was increased from 20 to 40% while increasing the CdO concentration for the prepared polymer nanocomposites. The T_d of PANI nanocomposites for all the three stages was increased gradually in accordance with the heating rates. The E_a for the three stages of degradation processes was determined using the non-isothermal kinetics model. The dc electrical conductivity of PANI nanocomposites was increased gradually while increasing the CdO concentration.

Compliance with ethical standards

Conflict of interest The authors declare that they have no conflict of interest.

Publisher's note: Springer Nature remains neutral with regard to jurisdictional claims in published maps and institutional affiliations.

References

- Seidel KF, Rossi L, Mello RMQ, Hümmel M, Melgen IM (2012) Vertical organic field effect transistor using sulfonated poly(aniline)/Aluminum bilayer as intermediate electrode. *J Mater Sci* 24:1052–1056
- Kumar V, Goyal PK, Mahendia S, Gupta R, Sharma T, Kumar S (2011) Tuning of refractive index and optical band gap of CR-39 polymer by heating. *Rad Eff Def Solids* 166:109–113
- Wan (2008) Conducting polymers with micro or nanometer structure. Tsinghua University Press, Beijing and Springer-Verlag GmbH, Berlin, Heidelberg
- Wallace GG, Spinks GM, Kane-Maguire LAP, Teasdale PR (2009) Conductive electroactive polymers. Taylor & Francis Group, LLC, Florida
- Jiang L, Li J, Xu F (2007) Synthesis and ferromagnetic properties of novel Sm-substituted Li,Ni ferrite-polyaniline nanocomposites. *Mater Lett* 61:109
- Srivastava S, Kumar S, Singh VN, Singh M, Vijay VK (2011) Synthesis and characterization of TiO₂ doped polyaniline composites for hydrogen gas sensing. *Int J Hydro Energ* 36:43–55
- Wei D, Ivaska A (2006) Electrochemical biosensors based on polyaniline. *Part A Chem. Anal* 51:39–52
- Cheng FY, Tang W, Li CS, Chen J, Liu HK, Shen PW, Dou SX (2006) Conducting poly(aniline) nanotubes and nanofibers: controlled synthesis and application in lithium/poly(aniline) rechargeable batteries. *Chem Eur J* 12:82–88
- Deshpande NG, Gudage YG, Sharma R, Vyas JC, Kim JB, Lee YP (2009) Studies on tin oxide-intercalated polyaniline nanocomposite for ammonia gas sensing applications. *Sens Actuat* 138:76–84
- Katz E, Willner I, Wang J (2004) Electroanalytical and bioelectroanalytical systems based on metal and semiconductor nanoparticles. *Electroanal* 16:19–44
- Balaz AC, Emric T, Russel T (2006) Nanoparticle polymer composites: where two small worlds meet. *Nanopart Sci* 314:7–10
- Chen X, Qi S (2017) Preparation and microwave absorbing properties of poly(aniline)/NiFe₂O₄/graphite nanosheet composites via sol-gel reaction and *insitu* polymerization. *J Sol-Gel Sci Technol* 81:824–830
- Bavastrello V, Carrara S, Ram MK, Nicolini C (2004) Optical and electrochemical properties of poly(o-toluidine) multiwalled carbon nanotubes composite Langmuir-Schaefer films. *Langmuir* 20:969–973
- Liu A, Bac LH, Kim BK, Kim JS, Kim JC (2013) Synthesis and characterization of conducting polyaniline-copper composites. *J Nanosci Nanotechnol* 13:7728–7733
- Ingle RV, Arote SA, Rajendra Prasad MB, Kadam VS, Mane RS, Inamuddin Mu, Naushad, Tabhane VA, Pathan HM (2014) Studies on facile synthesis of polyaniline/cadmium sulfide composites and their morphology. *High Perform Polym* 26:660–665
- Nagesa Sastry D, Revanasiddappa M, Basavraja C, Suresh T, Raghavendra SC (2013) DC conductivity studies of doped polyaniline tungsten oxide. *J Eng Mater Sci* 20:435–442
- Sravani C, Reddy KTR, Md. Hussain O, Reddy PJ (1996) Polycrystalline thin film CdO/CdTe solar cells. *J Solar Energy Soc India* 6:1–9
- Zhao Z, Morel DL, Ferekides CS (2002) Metal-organic chemical vapour deposition of thin films of cobalt on different substrates: study of microstructure. *Thin Solid Films* 413:203–211
- Aashis Roy S, Koppalkar R, Anilkumar MVN, Ambika P (2012) Studies of AC conductivity and dielectric relaxation behavior of CdO-doped nanometric polyaniline. *J Appl Polym Sci* 123:928–1934
- Mahalakshmi S, Alagesan T, Parthasarathy V, Tung KL, Anbarasan R (2018) Non-isothermal crystallization kinetics and degradation kinetics studies on barium thioglycolate end-capped poly(ϵ -caprolactone). *J Therm Anal Calorim* 135:3129–3140
- Selvi J, Mahalakshmi S, Parthasarathy V (2017) Synthesis, structural, optical, electrical and thermal studies of poly(vinyl alcohol)/CdO nanocomposite films. *J Inorg Organomet Polym* 27:1918–1926
- Tauc J, Grigorovici R, Vancu A (1966) Optical properties and electronic structure of amorphous germanium. *Physica Status Solidi* 15:627–637
- Jancirani A, Kohila V, Meenarathi B, Yelilarasi A, Anbarasan R (2016) Synthesis, characterisation and non-isothermal degradation kinetics of novel poly(mono ethylene glycol dimethacrylate-co-4-aminobenzoate). *Bull Mater Sci* 39:1725–1733
- Anbarasan R, Seethalakshmi M, Maria Franklin Dheepa A, Jayalakshmi T, Dhanalakshmi V (2013) Synthesis and characterization of CdO nanorod by Ultrasound assisted one pot method and its surface catalytic effect on poly(vinyl alcohol). *Ind J Sci* 2:121–123
- Aijie L, Luong Huu B, Ji-Soon K, Byoung-Kee K, Jin-Chun K (2013) Synthesis and characterization of conducting polyaniline-copper composites. *J Nanosci Technol* 13:7728–7733
- Aldwayyan AS, Jekhedab FM, Noaimi MA, Hammouti B, Hadda TB, Suleiman M, Warad I (2013) Synthesis and characterization of CdO nanoparticles starting from organometallic Dmphe-CdI₂ complex. *Int J Electrochem Sci* 8:10506–10514
- Wang Y, Liu M, Lu D, Zhang H (2019) Electrospun porous hybrid CuO/CdO nanofibers using carboxylic functionalized poly(arylene ether ketone)s as a template for glucose determination. *High Perform Polym* 31:570–579
- Almasi MJ, Fanaei Sheikholeslami T, Naghdi MR (2016) Band Gap study of Polyaniline and polyaniline/MWNT nanocomposites with *insitu* polymerization method. *Composites Part B* 96:63–68
- Yoffe AD (1993) Low-dimensional systems: quantum size effects and electronic properties of semiconductor microcrystallites (zero-dimensional systems) and some quasi-two dimensional systems. *Adv Phys* 42:173–262
- Rastogi AC, Sharma SN, Kohli S (2000) Size-dependent optical edge shifts and electrical conduction behaviour of RF magnetron

- sputtered CdTe nanocrystals:TiO₂ composite thin films. *Semicond Sci Technol* 15:1011
31. Ramna T, Alo D, Sayantani D, Akhilesh K, Sinha TP (2016) Dielectric relaxation of CdO nanoparticles. *Appl Nanosci* 6:175–181
 32. Ramesh P, Aashis S, Roy R, Koppalkar, Srikant E (2011) Electrical conductivity of polyaniline/NiZnO₃ composites: A solid state electrolyte. *Ferroelectrics* 423:77–85
 33. Eskizybek V, Avci A, Chowalla M (2011) Structural and optical properties of CdO nanowires synthesized from Cd(OH)₂ precursors by calcination. *Cryst Res Technol* 46:1093–1100
 34. Daikh S, Zeggai FZ, Bellil A, Benyoucef A (2018) Chemical polymerization, characterization and electrochemical studies of PANI/ZnO doped with hydrochloric acid and/or zinc chloride: Differences between the synthesized nanocomposites. *J Phys Chem Solids* 121:78–84
 35. Bauri K, Roy SG, Arora S, Dey RK, Goswami A, Madras G, De P (2013) Thermaldegradation kinetics of thermoresponsive poly (N-isopropylacrylamide-co-N,N-dimethylacrylamide) copolymers prepared via RAFT polymerization. *J Therm Anal Calorim* 111:753–761